

# Advanced Method for Detecting Irregularities in Concrete Beams Using IOT Data from Sensors

<sup>1</sup>Chandrashekara R S, <sup>2</sup>Prof. (Dr.) Khanna Samrat Vivekanand Omprakash  
CMR University

Chandrashekara.rs@cmr.edu.in

**Abstract**— The increasing reliance on state assessments in civil engineering has sparked extensive research into methods for damage detection based on structural vibrations. Modal parameters, such as natural frequencies and mode shapes, have gained significant attention due to their invariance across structures. These parameters provide a global perspective, meaning their variations can help identify damage without the need for sensor placement directly at the damaged site. This feature is a key advantage in structural health monitoring (SHM) systems. Integrating MEMS sensors into SHM frameworks holds great potential for long-term monitoring, particularly for large-scale infrastructures. This paper introduces an innovative anomaly detection technique that analyzes raw sequential data through a statistical approach to identify damage associated with tendon prestress loss. The technique leverages a distributed monitoring system consisting of six high-performance MEMS sensors. To validate the system, the first mode frequency is initially analyzed, and the method is then tested on acceleration data from a 240 cm beam under three distinct damage scenarios. The results demonstrate high accuracy in damage detection and show that the system can also localize the damage effectively.

**Keywords**— *Distributed monitoring system, structural health monitoring, MEMS sensors, frequency domain decomposition, anomaly detection.*

## I. INTRODUCTION

The significance of structural condition assessments in civil engineering has driven considerable research into developing advanced methods for damage detection, especially those utilizing vibration measurements. Modal parameters, including natural frequencies, mode shapes, and modal damping, have become critical indicators due to their invariance despite changes in the structure. These parameters reliably reflect the presence of damage as they vary with alterations in the structure's integrity. Additionally, the global nature of modal parameters enables damage detection without requiring sensor placement directly on the damaged area. Recent advancements in system identification techniques, such as output-only stochastic subspace algorithms, have strengthened the focus on modal parameters by offering numerically stable and reliable methods to determine these parameters experimentally from ambient excitations.

Structural health monitoring (SHM) plays a crucial role in ensuring the safety and longevity of structures by providing vital insights into their stress states and identifying potential

damage. SHM encompasses various techniques and technologies widely adopted in both aerospace and civil engineering sectors. In infrastructure asset management, ensuring the safety of structures is paramount, necessitating prompt and precise maintenance actions based on an in-depth understanding of the structural behavior, health conditions, and traffic load data. This is especially critical for bridges, where maintaining low vulnerability levels is essential for ensuring both safety and operational efficiency.

Damage and failure modes in complex systems like bridges can manifest in several ways. For prestressed concrete structures (PSCs), failure of the prestressing system is particularly critical, as it typically exhibits brittle behavior with little to no warning, potentially leading to catastrophic collapse. Prestressed concrete has been widely adopted for large-span structures, especially in bridge construction. However, this construction type is highly susceptible to degradation, and tendon rupture can result in fragile failure. Therefore, ongoing monitoring and maintenance of these structures are essential, requiring continuous inspection and monitoring. Early detection of damage is vital to prevent sudden failures, ensuring both user safety and reducing the financial burden of emergency repairs. While damage detection techniques for prestressed systems have been explored in the literature, a unified solution has not yet been established. Therefore, evaluating and developing methods that detect damage, particularly at early stages, remains necessary.

The integration of monitoring systems can help mitigate inconveniences to users and, in extreme cases, ensure their safety by enabling rapid interventions in the event of anomalies. This can be achieved through either direct intervention or by adopting a Bridge Management System (BMS) that optimizes maintenance activities while considering the structure's health. Additionally, these systems can be incorporated into broader frameworks that focus on goals such as reducing environmental impact or enhancing structural robustness.

This research primarily aims to develop a method for interpreting monitoring data that can be implemented in the workflows of entities responsible for managing reinforced concrete structures.

SHM systems are essential for providing reliable, real-time assessments of the monitored structures' conditions. Typically, SHM systems are categorized based on the type of data they collect: static and vibration monitoring. Static monitoring,

which tracks parameters like displacements, deformations, and rotations, is commonly used to monitor damage evolution. Although static methods have been explored for detecting tendon damage, they often require expensive measurement technologies such as fiber Bragg gratings or emerging systems still undergoing validation.

Recently, Micro-Electro-Mechanical System (MEMS) sensors have gained traction in SHM systems. MEMS sensors are compact, low-cost, and low-power devices that can accurately measure various physical parameters such as acceleration, strain, pressure, and temperature. Their integration into SHM systems offers several advantages, including improved data acquisition, processing capabilities, enhanced reliability, and reduced power consumption. MEMS sensors enable real-time monitoring of stress states, early damage detection, and predictions regarding the structural lifespan. In bridge applications, MEMS sensors have proven effective in continuously monitoring structural changes caused by external loads, traffic, or environmental factors. However, challenges such as noise and sensitivity to environmental changes require careful consideration. For example, random noise and bias drift can complicate error compensation and affect the long-term applicability of inertial MEMS sensors. These challenges necessitate advancements in sensor classification based on bias instability and random walk parameters.

Traditional SHM methods, such as strain gauges and wired sensor networks, are known for their reliability and precision. However, these methods often face challenges, including high installation costs, limited scalability, and vulnerability to environmental interference. MEMS technology presents a promising alternative, offering advantages such as compactness, high sensitivity, and wireless capabilities. While traditional accelerometers excel in high-frequency vibration monitoring, MEMS sensors are particularly effective in low-frequency applications and can easily integrate into wireless sensor networks. Recent innovations in MEMS technology have focused on advancements in smart sensors for SHM, embedded sensor improvements, and durability enhancements for high-temperature environments.

MEMS sensors combine mechanical and electrical components at the microscale to measure physical parameters like acceleration and displacement. Their working principles are based on changes in capacitance, which translate structural responses into electrical signals for further analysis. Their small size, low power requirements, and wireless capabilities make them ideal for deployment in challenging environments such as prestressed concrete structures. These features enable MEMS sensors to detect early signs of structural deterioration, such as crack propagation and shifts in modal frequencies. However, challenges such as temperature sensitivity and long-term degradation remain, which has prompted ongoing research into improving sensor durability and developing algorithms to mitigate environmental effects.

By analyzing the capabilities and limitations of MEMS sensors in SHM, particularly for prestressed concrete structures, this research highlights their potential to revolutionize modern infrastructure monitoring. The integration of MEMS-based solutions represents a significant advancement in SHM methodologies, offering scalable, cost-effective tools to ensure the safety and longevity of critical infrastructure.

Despite existing challenges, MEMS sensors have the potential to significantly enhance SHM systems. They offer efficient, accurate, and cost-effective solutions for structural monitoring and maintenance. Further advancements in MEMS technology and data analytics are expected to improve SHM capabilities, introducing novel approaches to structural monitoring and maintenance.

Vibration monitoring captures a structure's dynamic behavior under operational and ambient conditions using accelerometers or velocimeters. This data can be analyzed directly or used in Operational Modal Analysis (OMA) to determine the dynamic properties of a structure. Although this approach offers a global assessment of the structure, it may be less effective at detecting localized or early-stage damage, such as tendon failures, which might not significantly affect dynamic properties.

The primary aim of this research is to develop and validate an anomaly detection method using MEMS-based sensors to monitor tendon integrity in prestressed concrete structures, grounded in vibration-based methods that can detect structural changes even when the sensors are not located near the damage.

## II. THE PROPOSED METHOD

Early detection of damage in prestressing systems is crucial for ensuring the safety and reliability of prestressed concrete structures (PSCs). The methodology proposed in this paper employs a similarity analysis of acceleration time histories to differentiate between healthy and damaged structural states. The method consists of two phases: the calibration phase, where reference data from the undamaged structure are collected, and the operational phase, where new data are analyzed for damage detection.

During the calibration phase, multiple acceleration time histories are gathered to represent the dynamic behavior of the structure in its undamaged state. These data are used to define baseline conditions, serving as the reference for anomaly detection. The number of accelerometers installed on the structure is denoted by  $K$ , and the number of histories acquired from each accelerometer during calibration is denoted by  $N$ . The acceleration data from the sensors form a reference matrix of acceleration time histories:

$$A_{ccr} = \begin{pmatrix} A_{ccr,1,1} & \cdots & A_{ccr,1,N} \\ \vdots & \ddots & \vdots \\ A_{ccr,K,1} & \cdots & A_{ccr,K,N} \end{pmatrix} \quad (1)$$

The similarity between time histories is measured using a function such as the Minimum Jump Cost (MJC), which calculates the cost of transitioning from one-time history to another. The similarity index (SI) matrix is constructed by comparing each time history with others from the same sensor:

$$SI_{i_0,j_0} = \frac{1}{N-1} \sum_{i \neq i_0} S_{im}(A_{ccr,i_0,j_0}; A_{ccr,i,j_0}) \quad (2)$$

To detect anomalies, a control chart approach is used. The mean ( $\mu$ ) and standard deviation ( $\sigma$ ) of the SI matrix are computed, and threshold values are defined as:

$$\mu \pm \lambda\sigma \quad (3)$$

Here,  $\lambda=3$  is used, based on Chebyshev's theorem, which states that the probability of observing values outside these thresholds is at most 11%. These thresholds define the baseline for detecting anomalies during the operational phase. As new acceleration data are collected, the similarity index is recalculated for the new measurements:

$$SI_{new,i_0,j_0} = \frac{1}{N} \sum_i S_{im}(A_{new,i_0,j_0}; A_{ccr,i,j_0}) \quad (4)$$

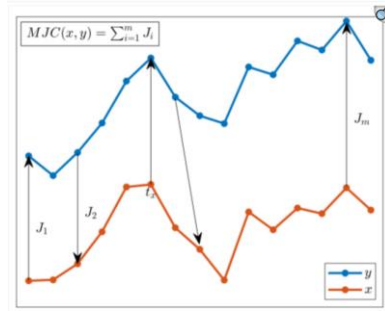
If any value in the new SI matrix falls outside the defined thresholds, the system triggers an anomaly alert. When more than 11% of the values are outliers, the system detects an anomaly in the structural behavior.

The MJC function evaluates the cost of transitioning between two sequences,  $x$  and  $y$ , and is calculated as the sum of the minimum costs for each jump:

$$MJC(x, y) = \sum_{i=1}^m J_i \quad (5)$$

where  $J_i$  represents the cost of the jump between data points in sequences  $x$  and  $y$ .

**Minimum Jump Cost description.**

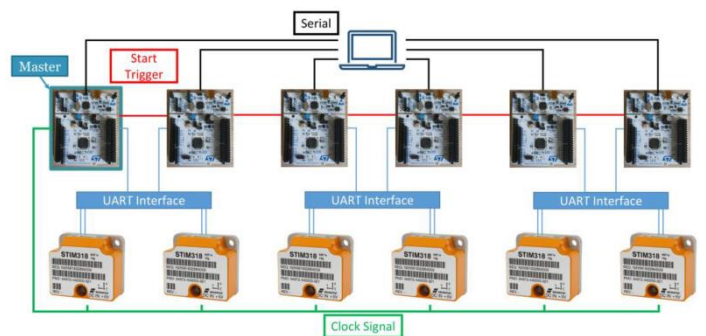


In this work, the Minimum Jump Cost (MJC) measure is adopted as the criterion for comparing two distinct time histories, i.e., for evaluating the distance between them. However, alternative approaches can be employed for defining the distance measure. In fact, Equation (2) introduces a generic notation,  $S_{im}$ , to represent any arbitrary similarity measure, emphasizing the flexibility of the proposed method.

III. SYSTEM ARCHITECTURE

The data acquisition system, as depicted in Figure 2, is based on MEMS sensors and consists of six high-performance inertial sensors provided by Sensoror™ (Skoppum, Norway), along with six microcontrollers from STMicroelectronics™ (Geneva, Switzerland). In this setup, the STM32F446RE microcontrollers collect data from the STIM318 sensors via the UART protocol. To enable seamless communication, an interface between the RS422 and UART protocols is established using the SN75C1167 chip from Texas Instruments (Dallas, TX, USA), allowing the microcontrollers to effectively acquire data through UART.

**System architecture based on six high-grade MEMS sensors.**



STIM318 sensors are configured to sample data at a frequency of 2 kHz, with the triggering frequency set to 250 Hz. This configuration ensures that the average delay between the data request and actual sampling is limited to 250  $\mu$ s. Additionally, the Master microcontroller generates a start signal, which is captured by the other microcontrollers to synchronize the initiation of the data acquisition process. The collected data are then transmitted to a PC, where they are used to trigger

acquisition by the Master and facilitate data collection from all microcontrollers via serial communication.

The architecture of this system was carefully selected based on several important factors that enhance its effectiveness in structural health monitoring applications. Firstly, the integration of high-performance sensors and microcontrollers ensures the system can meet the demands of accurate data collection. The STIM318 sensor, capable of high-frequency data acquisition at 2 kHz, offers a low noise density of 0.015  $m/s/\sqrt{hr}$ . Paired with the STM32F446RE microcontroller, which features an Arm Cortex-M4 processor running at 180 MHz, the system efficiently processes and manages the acquired data. Another key consideration was the need for precise synchronization, which is crucial for structural monitoring. The synchronization between the sensors and microcontrollers is achieved via an external clock and the start signal from the Master microcontroller, reducing delays and improving data reliability. Communication reliability was also a priority, and the use of an RS422-to-UART interface ensures efficient and robust data transmission. Finally, the modular and scalable nature of the system was essential, allowing it to adapt to various structural elements and incorporate additional sensors if necessary. The system is also designed for integration with Internet of Things (IoT) protocols, ensuring compatibility with future SHM applications.

#### IV. MEASUREMENT SETUP

The proposed methodology was validated through an experimental case study involving a prestressed concrete joist, a common structural element used in floor construction. The joist tested in the study had a length of 240 cm and featured a T-shaped cross-section with a height of 10 cm, a major base width of 12 cm, and a minor base width of 5 cm. The reinforcement configuration consisted of three prestressing tendons placed in the lower section of the joist and one tendon in the upper section, with each tendon having a cross-sectional area of 12 mm<sup>2</sup>. The joist was constructed using C45/55 grade concrete, which has a cylindrical compressive strength ( $f_{ck}$ ) of 45.65 N/mm<sup>2</sup> and an elastic modulus (EEE) of 36,416.11 N/mm<sup>2</sup>. The tendons were made of harmonic steel, with a characteristic yield stress ( $f_{p(1)k}$ ) of 1670 N/mm<sup>2</sup> and a characteristic ultimate tensile strength ( $f_{ptk}$ ) of 1860 N/mm<sup>2</sup>. A detailed representation of the joist's cross-section is shown in Figure 3, and the concrete and tendon properties are provided in Table 1.

#### Depiction of the joist section and tendon layout.

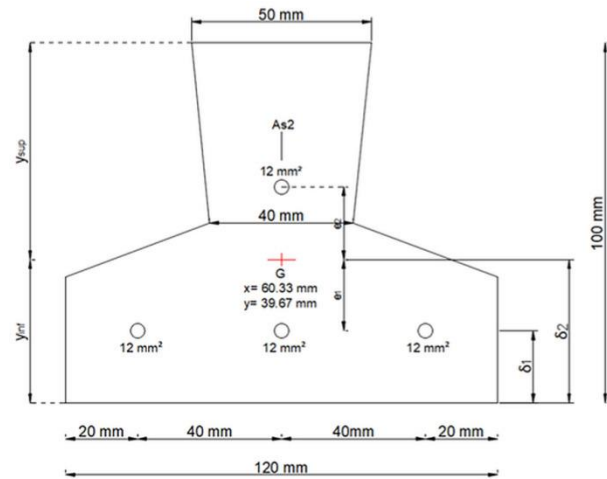
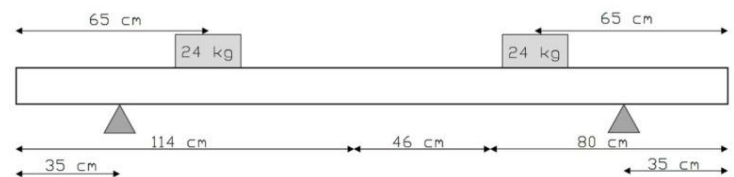


**Table 1. Characteristics of concrete and tendons of harmonic steel.**

Feature	Dimension	Value
$f_{ck}$	MPa	45.65
$E_c$	MPa	36,416.11
$E_s$	MPa	201,000
$f_{ptk}$	MPa	1860
$f_{p(1)k}$	MPa	1670

The experimental setup, shown in Figure 4, consisted of positioning the joist specimen on two symmetrical vertical supports, each placed 35 cm from the ends of the beam. To replicate loading conditions, two 24 kg masses were positioned 65 cm from the respective ends of the beam, ensuring that the load was evenly distributed across the structure.



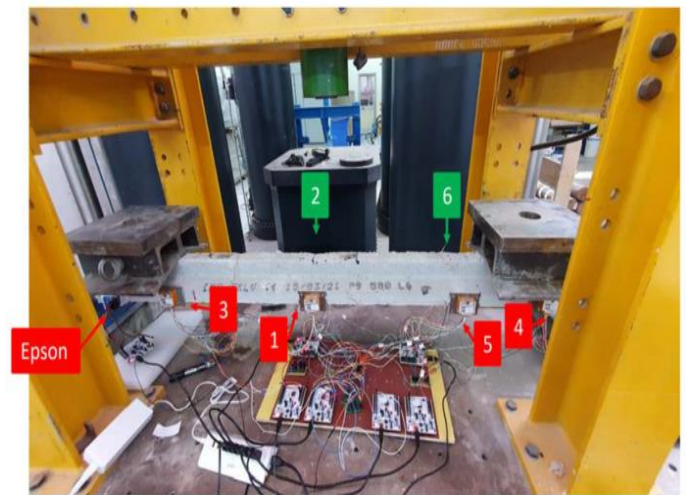
#### Setup for the experiments.

The proposed monitoring system was preliminarily assessed through a comparison with measurements taken from a low-noise MEMS sensor, the EPSON M-A352 accelerometer, which served as the reference system [36]. Data acquisition for the reference system was managed by an additional microcontroller that generated the clock signal and acted as an interface between the sensor and the PC. Synchronization between the proposed monitoring system and the reference system was achieved through a digital start signal transmitted from the Master microcontroller.

The sensors were arranged in two different configurations:

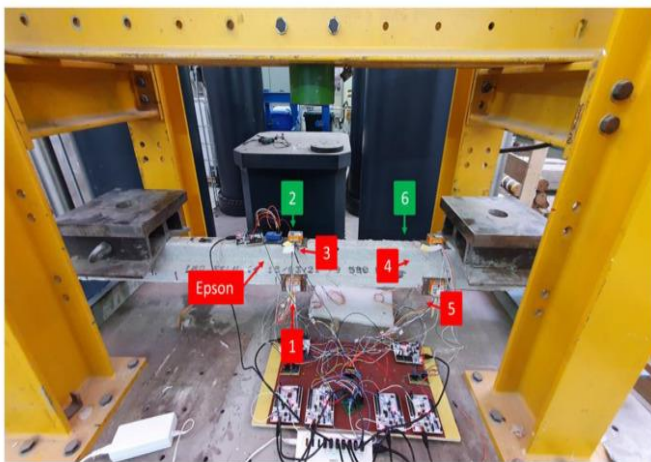


1. **Parallel Configuration:** In this setup, the STIM sensors were placed in two sections, with three sensors in each section. The first section was located 114 cm from the left end of the beam, and the second was positioned 160 cm from the left end. In each section, one STIM sensor was placed on the front side, one on the rear side, and one on the top side. The EPSON sensor was placed on the top side of the beam, 110 cm from the left end, near STIM sensor 3. The arrangement of these sensors is shown in Figure 5.
2. **Longitudinal Configuration:** In this configuration, four STIM sensors and the EPSON sensor were positioned on the front side of the beam, while two STIM sensors were placed on the rear side. A visual representation of this arrangement is provided in Figure 6.



Optimizing the layout of accelerometers is a key area of research in structural health monitoring (SHM). Numerous studies have proposed various methods and strategies for determining the ideal sensor placement to enhance detection capabilities and improve the identification of a structure's dynamic properties [37]. While determining the optimal sensor placement is beyond the scope of this paper, the authors tested two different configurations to assess their effectiveness in dynamic identification. For the damage detection analysis, however, only the parallel configuration was used, as it offered better sensitivity to off-center damage, such as a clipped tendon, which could lead to changes in internal stress and beam deflection.

**Distributed monitoring system of six STIM318 sensors (highlighted in red and green colors for front and back, respectively) in parallel configuration. Figure No.5**



**Distributed monitoring system of six STIM318 sensors (highlighted in red and green colors for front and back, respectively) in longitudinal configuration. Figure No.6**

## V. SYSTEM CHARACTERIZATION

**Measurement Synchronization:** The distributed monitoring system was first evaluated using controlled displacements in a single direction to assess the synchronization of the acquired acceleration signals (Figure 7). During this evaluation, the correlation between the signals was examined, and the outcome of combining two signals is shown in Figure 8.

**Figure No.7 Comparison of acceleration measurements of all sensors under controlled displacements in one direction.**

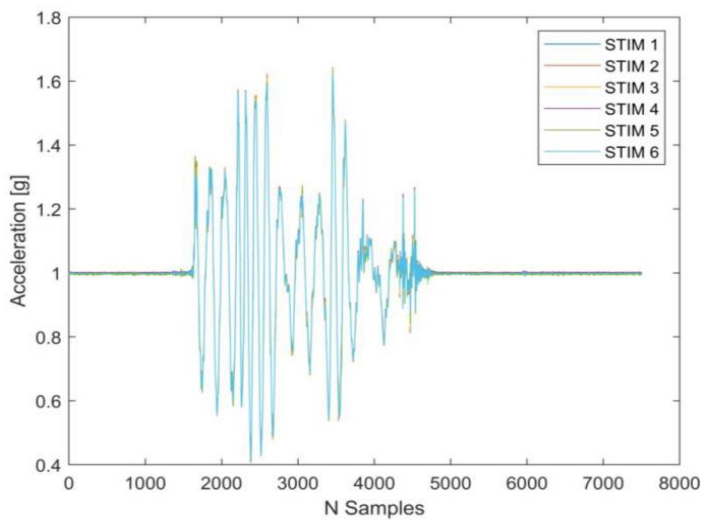
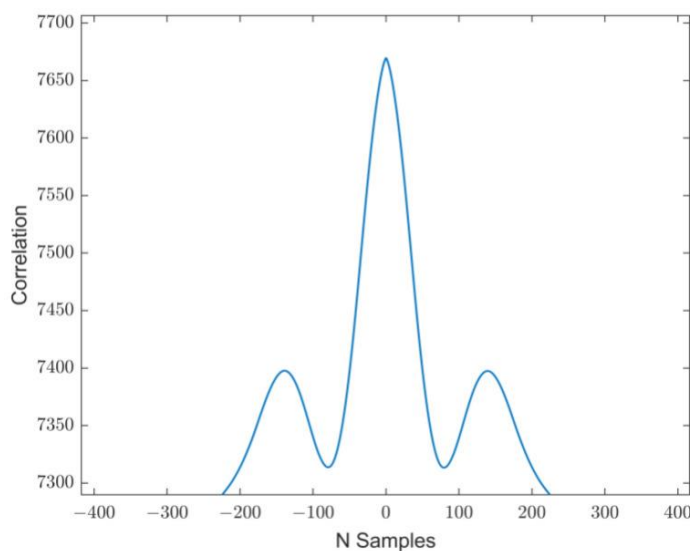


**Figure No.8 Correlation of two acceleration measurements.**



The cross-correlation between two acceleration signals was computed using MATLAB's `xcorr` function (version: 2024b). The x-axis represents the lag in terms of sample shifts (N samples), while the y-axis shows the correlation values. The peak of the correlation occurs at lag = 0, indicating a high degree of synchronization between the two signals, with no apparent time delay. Furthermore, the symmetrical shape of the curve suggests that the signals are temporally aligned without significant phase shifts. The side lobes surrounding the main peak indicate secondary correlations, which arise from periodic or repeating patterns in the signals. This result confirms that the synchronization between the two signals is valid, reflecting shared, similar dynamic responses.

In addition to the synchronization analysis, the time required for data retrieval from the sensor, along with the transmission and reception times for the acquisition start signal, was

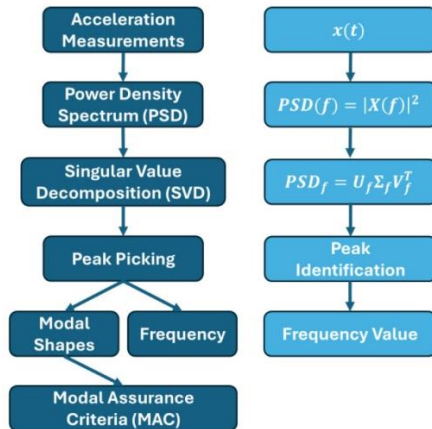
measured. The average data retrieval time was found to be 0.54 ms, with a standard deviation of approximately 500 ns, while the transmission and reception times were about 40 ns each. The internal timers of the microcontroller were also used to measure the actual sampling rate, which was determined to be 4 ms.

**Performance Evaluation:** -Frequency Domain Decomposition (FDD) is a valuable output-only method used to identify the vibration frequencies and corresponding modal shapes of a structural system based on acceleration data recorded from the structure. This technique operates on the principle that the eigenvectors, which represent the vibration modes, form a basis due to their linear independence. As a result, any displacement in the system can be represented as a linear combination of these eigenvectors, allowing the decoupling of mode components. This property is particularly useful when analyzing the system's response at each accelerometer placement or when examining the Power Spectral Density (PSD) of the accelerometer's history using Singular Value Decomposition (SVD) of the matrix defined for each frequency  $\omega$  [38].

The FDD method utilizes frequency response functions (FRFs) to extract the eigen periods, damping, and modal deformations of the structure. Fourier transforms are employed to convert the differential equations governing the dynamic behavior of the structure into a system of algebraic equations, simplifying their resolution.

Figure 9 presents a flowchart outlining the data processing steps using the FDD technique, along with its mathematical description. Initially, the PSDs are estimated through Fourier transforms of the acceleration signals,  $x(t)$ , which represent the acceleration measurements. The resulting PSD matrices, one for each frequency  $f$ , are then decomposed into singular values. In this decomposition,  $Uf$  and  $Vf$  represent the singular vectors, while  $\Sigma f$  denotes the singular values. These singular values correspond to the degrees of the structural system, and the singular vectors provide insights into the modal form. Vibration modes are identified based on the graphical representation of the singular value spectrum, specifically at the resonance peaks. Natural frequencies are identified using the peak-picking method, where each peak corresponds to a singular value, which is matched with a singular vector. The suitability of attributing a frequency to a specific vibration mode is evaluated using the Modal Assurance Criteria (MAC) [39,40]. It is critical to assess the frequency in order to identify the component of interest. To validate the proposed system, the results were compared with those obtained using Artemis Modal Pro software (version 8) and the reference system.

**Figure No.9 FDD Technique Flow Chart**



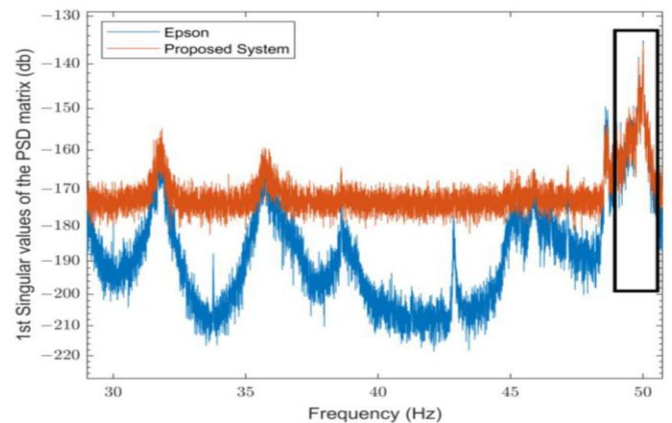
In particular, Table 2 shows the frequencies obtained by means of the software, which identifies that the first mode exhibits frequencies of about 50 Hz and 53 Hz in the absence of an applied load for the parallel and longitudinal configurations, respectively, while frequencies of about 40 Hz and 41 Hz for the parallel and longitudinal configurations, respectively, are observed with an applied load, a result that is also evident in the finite element model. For the unloaded beam, the discrepancies between the FEM and Artemis, ranging between 5% and 10%, likely stem from minor differences in the boundary conditions and material properties inherent to the theoretical and experimental Setups.

	[Hz]	Parallel Config. [Hz]	Longitudinal Config. [Hz]
Unloaded	55.16	50.68	53.83
Loaded	34.10	40.87	41.62

On the other hand, in the presence of a load on the analyzed beam, the differences are slightly more pronounced, at around 20%. This variation can be attributed to the influence of the applied load, which affects the stiffness and stress distribution. These factors are more accurately reflected in the experimental conditions than in the FEM's idealized assumptions. Once the first mode had been evaluated through the FEM analysis and using Artemis Modal Pro software, the outcomes obtained by the proposed system and the reference system were then examined around the frequency of interest, as shown in Figure 10 and Figure 11 for the parallel configuration in the absence of an applied load and in the presence of an applied load, respectively. Both systems correctly identify the frequency of the first mode, with values equal to 50.01 Hz for the reference system and equal to 50.01 Hz for the proposed system for an unloaded beam and values equal to 40.29 Hz for the reference system and equal to 40.18 Hz for the proposed system in the loaded case. Furthermore, both systems demonstrate a variation

in the frequency of the first mode of the beam from about 50 Hz to 40 Hz when a load is applied, i.e., in dynamic conditions.

**Figure 10. First mode of the parallel configuration without applied load.**



VI. RESULTS

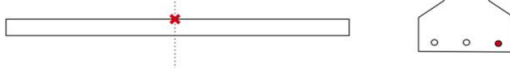


The experimental campaign consisted of four tests (T0–T3), with each aiming to evaluate both the identification system's performance under an increasing damage severity and the effectiveness of the proposed methodology for identifying tendon failure. All of the experimental tests involved the acquisition of 146-time histories of 600 s in ambient conditions. The damage was induced by creating narrow, deep cuts near the tendons, as shown in Figure 12. In each test, the system's abilities to detect anomalies and correlate the number of alerts with the damage extent were assessed. Test T0 served to confirm that the system does not trigger alerts in response to minor variations in the positions of the masses or sensors, while tests T1 to T3 assessed the system performance under the conditions of progressively increasing damage. This study further sought to explore the potential correlation between the number of alerts generated and both the extent and location of the damage. Figure 13 provides a detailed overview of the damage patterns applied in each experiment. For this campaign, the similarity function introduced previously, in the context of time-series analysis, was utilized.

**Figure 12. Example of cuts near the tendons.**





**Figure 13. Experimental damage patterns adopted.**

Test	Structural Condition
T0	Undamaged structural before and after the dismounting and remounting of the sensors.
T1	Single local damage at the mid-span of a lateral tendon. (D1) 
T2	Local damages at the mid-span of both lateral tendons, single local damage affecting one of the lateral tendons close to the beam's support. (D2) 
T3	Local damages at the mid-span of all bottom tendons, single local damage affecting one of the lateral tendons close to the beam's support. (D3) 

The initial test evaluates the methodology's sensitivity to minor alterations in the experimental setup. Specifically, the response of the undamaged joist is analyzed by disassembling and reassembling the sensors to determine how slight modifications in the sensor-structure configuration affect the system. According to Chebyshev's theorem, the control chart probability of exceeding the set thresholds is at most 11%, meaning anomalies can be detected as follows:

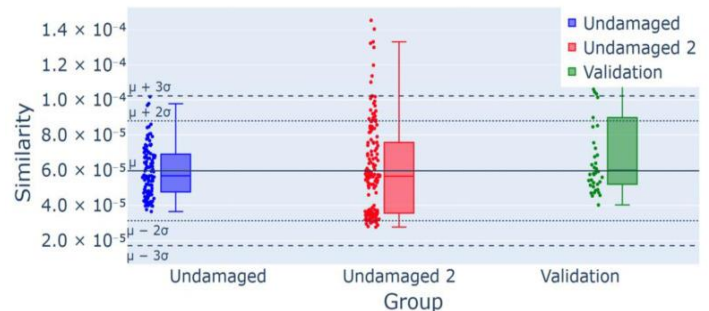
$$\frac{\text{Number of outliers}}{\text{Number of samples}} > 0.11 \tag{6}$$

The results of the outlier analysis are shown in the control charts, which depict the performance across three data groups: training, testing, and validation. The training data, shown in blue, are used to establish the control chart thresholds. The validation data, represented in green, come from the undamaged structure's measurements collected during the training phase. The testing data, shown in red, correspond to the testing group.

Figure 14 illustrates the T0 damage detection analysis, presenting the control chart based on the similarity index under undamaged conditions. The chart includes data for the calibration-free validation measurements (green) and those obtained after sensor disassembly and reassembly (red). According to Figure 14, the number of outliers detected in the "Undamaged 2" dataset is 8, resulting in an occurrence frequency of 5.5% for 146 five-minute time histories (approximately 12 hours). This value is below the 11%

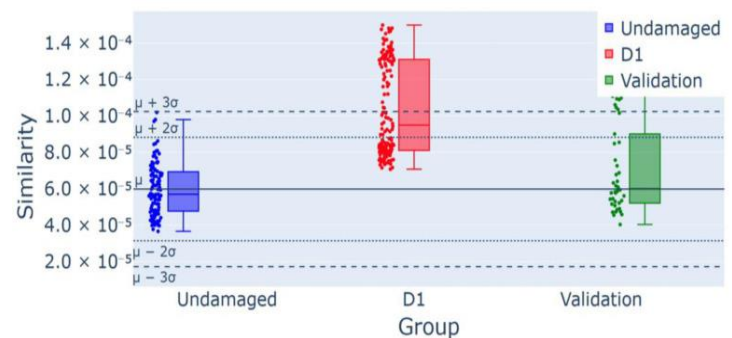
threshold required to trigger an alert, demonstrating the robustness of the system to minor sensor adjustments.

**Figure 14. Control chart for experiment T0 for sensor arrangement: 8/146 (5.5%) outliers for the group Undamaged 2, confirmed using the validation group as a part of the undamaged data.**



The results from test T1, with the D1 damage scenario, are shown in Figure 15, where the similarity index computed for the time histories under D1 conditions is represented in red. The methodology detected 64 outliers, approximately 43.8% of the dataset, which exceeded the 11% threshold, leading to anomaly detection and indicating structural changes.

**Figure 15. Control chart for experiment T1 for D1 damage detection: 64/146 (43.8%) outliers for the group D1, confirmed using the validation group as a part of the undamaged data.**



- In advanced damage scenarios (T2 and T3), as shown in Figure 16 and Figure 17, the control charts visually illustrate an increased number of outliers for damage scenarios D2 and D3, with the alerts totaling 80 and 146, respectively, corresponding to 54.8% and 100% of the newly collected measurements. These findings confirm the detection of anomalies in each case.
- Regarding T2 and T3, the control charts in Figure 15 and Figure 17 already visually highlight a considerable number of outliers that result in the detection of an anomaly. In cases D2 and D3, there are 80 and 146 alerts, respectively, which consist of 54.8% and 100% of the sample of new measurements.



- The system successfully detected damage in all scenarios (D1–D3) and demonstrated a direct correlation between the damage severity and the percentage of outliers. As the damage intensified, the percentage of outliers rose, reaching 100% in the most severe cases. Therefore, referring only to the investigated scenarios and adopting the 11% outlier threshold gives an overall accuracy of 100% because the presence or absence of damage was correctly detected in all four investigated scenarios.

**Figure 16. Control chart for experiment T2 for D2 damage detection: 80/146 (54.8%) outliers for the group D2, confirmed using the validation group as a part of the undamaged data.**

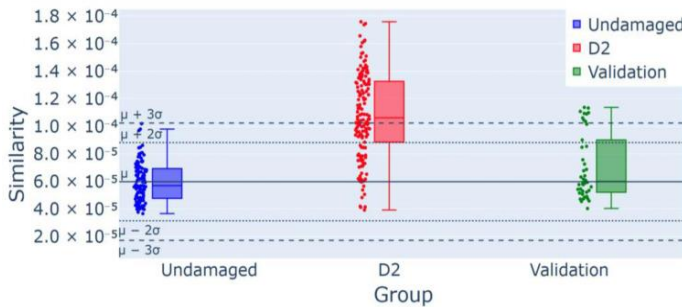
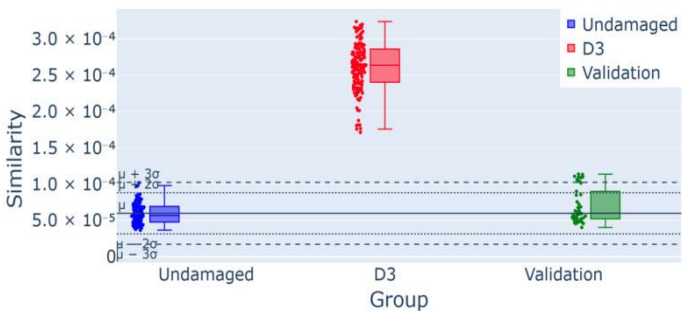


**Figure 17. Control chart for experiment T3 for D3 damage detection: 146/146 (100%) outliers for the group D3, confirmed using the validation group as a part of the undamaged data.**



A further analysis involved the detection of damage localization using a sensor-based analysis; in particular, this was conducted on test T2 by evaluating each sensor individually. Figure 18 shows that sensor 6, located near the damage, registered a higher number of outliers compared to sensor 5 (Figure 19), positioned on the opposite face of the same section. This suggests that the methodology may effectively localize damage within the structure. All of the experiments and the results they achieved are reported in Table 3, where the damage scenarios, key objectives, number of alerts, outlier percentages, and observations have been summarized.

**Figure 18. Control chart for experiment T2 for D2 damage detection from sensor 6 (S6): 99/146 (67.8%) outliers for the group D2-S6, confirmed using the validation group as a part of the undamaged data.**

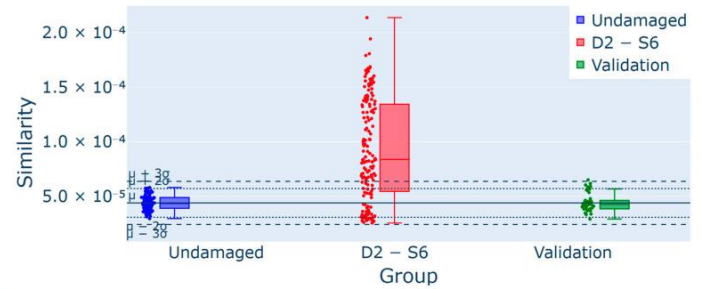
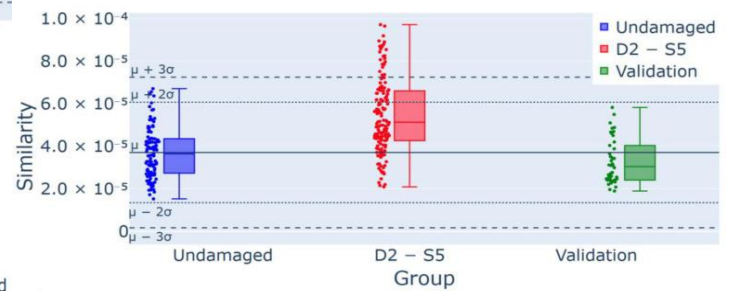


**Figure 19. Control chart for experiment T2 for D2 damage detection from Sensor 5 (S5): 25/146 (17.1%) outliers for the group D2-S5, confirmed using the validation group as a part of the undamaged data.**



## VII. CONCLUSION

This study presents a distributed monitoring system based on MEMS sensors for structural health monitoring (SHM). The system's performance was preliminarily evaluated by comparing it with a low-noise sensor in a case study involving both unloaded and loaded prestressed concrete beams. The goal was to validate the proposed method, which was then compared with results from analytical and finite element models. The authors proposed a damage detection framework for prestressed concrete (PSC) beams, leveraging direct analysis of acceleration time histories obtained from a reliable and cost-effective SHM system. Damage detection in prestressed bridge systems is a critical challenge in structural engineering, as accurate assessments are essential for ensuring transportation safety. The methodology for identifying damage in PSC elements involves analyzing acceleration time histories using a similarity index to detect anomalies. Thresholds for this analysis are established using a reference dataset, and any measurements exceeding these thresholds are classified as outliers. According to Chebyshev's theorem, a structural anomaly is identified if the outliers exceed 11% of the total measurements; otherwise, the values are considered part of the normal distribution variance.

The methodology was experimentally validated using a reinforced concrete joist in four tests. The first test evaluated the system's resilience to false positives, showing no anomalies when the sensor configuration was slightly adjusted. The following tests focused on damage detection, with outlier percentages ranging from 43% to 100%, demonstrating strong accuracy in detecting damage and a clear correlation between outlier frequency and damage intensity. The final test, which analyzed data from individual sensors, indicated the potential for damage localization using single-sensor data, as sensors located near the damage exhibited a higher number of outliers.

In summary, the proposed methodology exhibited robust performance in detecting various levels of damage under controlled conditions. However, its effectiveness relies on a comprehensive baseline dataset and an adequate number of sensors for multiscale damage detection. Future work will

explore alternative similarity metrics and machine learning techniques to address environmental variability and further improve damage detection capabilities.

#### VIII. REFERENCE

- [1]. IEEE Xplore – Prediction of Cement Strength using Machine Learning Approach. This paper discusses various machine learning models, including Gradient Boosting, for predicting cement strength. Read here (Prediction of Cement Strength using Machine Learning Approach | IEEE Conference Publication | IEEE Xplore).